High-Resolution Study of X-Ray Resonant Raman Scattering at the *K* Edge of Silicon

J. Szlachetko,[1,3] J.-Cl. Dousse,[1] J. Hoszowska,[2] M. Pajek,[3] R. Barrett,[2] M. Berset,[1] K. Fennane,[1]
A. Kubala-Kukus,[3] and M. Szlachetko[1]

[1]*Department of Physics, University of Fribourg, CH-1700 Fribourg, Switzerland*
[2]*European Synchrotron Radiation Facility (ESRF), F-38043 Grenoble, France*
[3]*Institute of Physics, Swietokrzyska Academy, 25-406 Kielce, Poland*

We report on the first high-resolution measurements of the *K* x-ray resonant Raman scattering (RRS) in Si. The measured x-ray RRS spectra, interpreted using the Kramers-Heisenberg approach, revealed spectral features corresponding to electronic excitations to the conduction and valence bands in silicon. The total cross sections for the x-ray RRS at the $1s$ absorption edge and the $1s$-$3p$ excitation were derived. The Kramers-Heisenberg formalism was found to reproduce quite well the x-ray RRS spectra, which is of prime importance for applications of the total-reflection x-ray fluorescence technique.

The x-ray Raman scattering is a second-order process of photon-atom interaction in which a core electron is excited into an unoccupied state above the Fermi level by absorption of a photon. This intermediate ''virtual'' state of the neutral atom decays then radiatively, the initial core hole being filled by another inner-shell electron. The energy of the ''scattered'' photon $\hbar\omega'$ is given by $\hbar\omega' = \hbar\omega - |B_f| - \epsilon$, where $\hbar\omega$ stands for the energy of the incoming photons, B_f is the binding energy of the inner-shell hole in the final state, and ϵ is the energy of the excited core electron above the Fermi level. The cross section for Raman scattering is generally extremely small compared to elastic Rayleigh scattering. However, if the energy of the incoming photon is close to an absorption threshold, the Raman process is resonantly enhanced and its cross section increases dramatically. Pioneering works on the x-ray resonant Raman scattering (RRS) using x-ray tubes were performed in the 1970s by Sparks [1] and synchrotron radiation by Eisenberger *et al.* [2].

Because of its resonant character, the x-ray RRS is a powerful method to study the electronic structure of solids, being complementary to the x-ray absorption techniques based on the first-order process. High-resolution x-ray RRS measurements represent a novel experimental tool to probe unoccupied states in silicon, giving thus deeper insight into the electronic structure of this important material for semiconductor industry.

On the other hand, it has been realized that the RRS process sets the limits for application of the total-reflection x-ray fluorescence (TXRF) method [3] for measuring very low concentrations of light element impurities on the surface of Si wafers. For instance, several experiments [4,5] have shown that the detection limit of Al impurities on the Si surface is limited by the presence of RRS x rays. In fact, for incident photon energies tuned below the Si *K*-absorption edge to avoid the intense Si *K* fluorescence x-ray line, the RRS structure of Si is indeed overlapping with the Al *K* x-ray fluorescence peak. Since the TXRF technique combined with intense synchrotron x-ray sources offers new possibilities for detection of light elements in ultraclean silicon, precise knowledge of the x-ray Raman scattering in silicon is therefore crucial for applications of the TXRF technique in the semiconductor technology. By now, only theoretical predictions [6–10] have been available for the RRS structure in silicon. However, to be used for reliable estimations of the detection limits of the TXRF method for light element impurities in silicon, these calculations needed experimental verification.

In this Letter we report on the first high-resolution measurements of the resonant x-ray Raman scattering in silicon, which yielded detailed shapes of the x-ray RRS spectra for TXRF applications. We also demonstrate that both the continuum and bound states close to the threshold can be probed in silicon by means of the RRS technique.

The RRS x-ray spectra were measured at the ESRF beam line ID21 by means of high-resolution x-ray spectroscopy, using a von Hamos Bragg-type curved crystal spectrometer [11] with an energy resolution of about 0.9 eV. The photon beam delivered by the undulator was monochromatized by means of two 20 Å Ni/B_4C multilayers and the residual higher-energy photons were suppressed with a Ni mirror. The monochromator was calibrated by measuring in the fluorescence mode the Al and Si *K*-absorption edges. Depending on the energy, 10^{12}–10^{13} incident photons per second with a FWHM energy resolution of ~6 eV were obtained on the sample, which represented a good compromise between an acceptable beam energy resolution and high enough beam intensity to investigate the weak RRS process. For all measurements the angle between the incoming beam and the target surface was set to 20°. Test-measurements performed at smaller incident angles showed RRS yields too poor to be measured in reasonable collecting times by means of high resolution. A 1 mm thick solid polycrystalline Si sample with a purity better than 99.99% was used.

The measured Si RRS x-ray spectra for beam energies tuned down to −50 eV below the 1s absorption edge are shown in Fig. 1(a), while those measured at energies tuned across the absorption edge, from −6 eV up to +4 eV with 2 eV steps, are presented in Fig. 1(b). As shown, the spectra consist of two components, a broad and asymmetric RRS structure whose position varies with the beam energy and a narrow Si $K\alpha$ fluorescence line which occurs for all beam energies at 1740 eV. The two components are well separated for beam energies smaller by about 10 eV than the Si 1s edge [Fig. 1(a)] but are overlapping for energies close to the edge [Fig. 1(b)]. The x-ray resonant Raman scattering investigated in the present experiment is due to the excitation of a 1s electron into the continuum (1s-εp) accompanied by a quasisimultaneous transition of a 2p electron to the 1s level. The RRS x-ray spectra have very long low-energy tails due to the Lorentzian shapes of the involved atomic levels and sharp high-energy cutoffs. The position of the cutoffs is given by $\hbar\omega' = \hbar\omega - |B_f|$ since $\epsilon = 0$ and is therefore shifted towards higher energies when the beam energy increases. The Si $K\alpha_{1,2}$ fluorescence line (2p-1s transition) results from the photoionization of 1s electrons by photons from the high-energy tail of the beam energy distribution. For this reason, the intensity of the Si $K\alpha_{1,2}$ fluorescence line for incident photon energy below the K edge diminishes rapidly and saturates above the absorption edge.

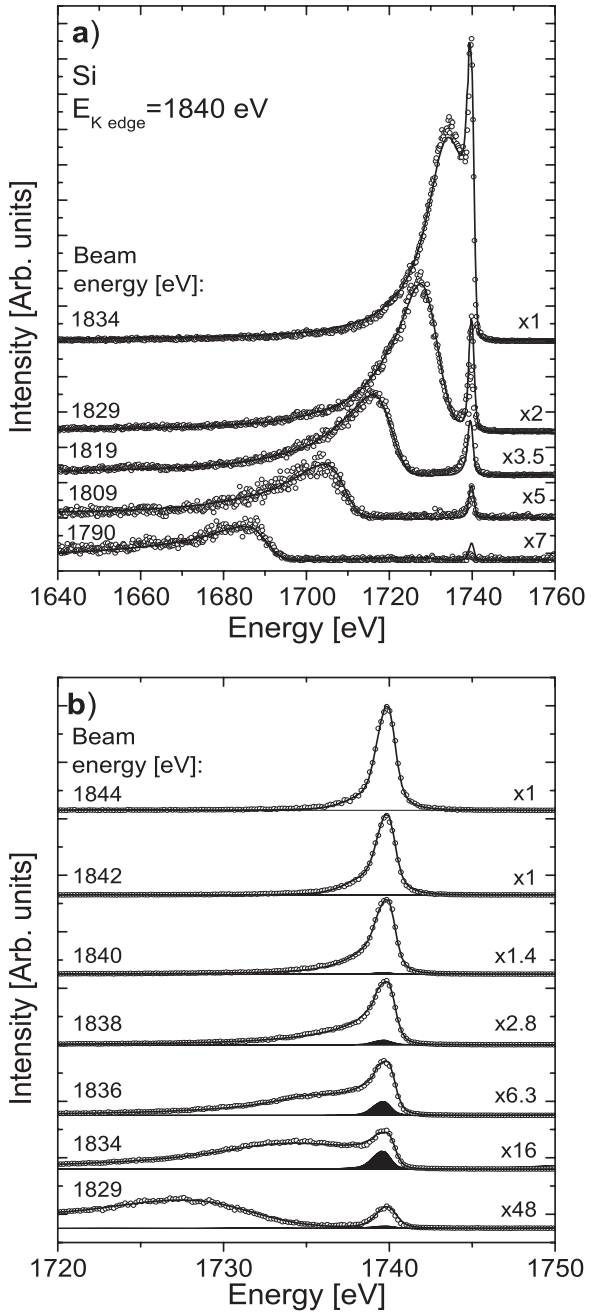

FIG. 1. High-resolution RRS x-ray spectra of Si for incident beam energies tuned (a) below the 1s absorption edge and (b) across it. The open circles represent the measured spectra, the solid black lines the theoretical predictions comprising both the continuum and discrete excitations. The filled areas in (b) stand for the predictions corresponding to the discrete excitations. For comparison, the spectra measured at 1829 and 1834 eV are presented in (a) and (b).

In order to understand the shapes of the observed spectra, calculations of the x-ray resonant Raman scattering around the K absorption edge were performed within the second-order perturbation theory using the Kramers-Heisenberg formula [7–9]. A more detailed description of these calculations can be found in [10]. The x-ray RRS profiles were computed assuming the excitation of a 1s electron into the continuum (above the Fermi level) and a 2p vacancy in the final state. The binding energies and natural widths of the 1s and 2p levels were taken from Refs. [12,13], respectively. The oscillator strength distributions $dg_{1s}/d\omega$ (see Ref. [10]) for silicon, needed in the Kramers-Heisenberg approach, were derived from the experimental RRS x-ray spectra in a self-consistent way (see Ref. [14]) by exploiting the fact that the RRS structure measured for different beam energies is determined by a common $dg_{1s}/d\omega$ function. In fact, the oscillator strength distributions extracted from the data for different energies were found to be very similar, so that the average of these distributions was chosen for $dg_{1s}/d\omega$ in the calculations of the theoretical RRS profiles. The beam energy distribution, which was derived from the above mentioned Si K absorption edge measurement, was found to be well reproduced by a Gaussian with a FWHM of 6.1 eV and a small Lorentzian contribution (8%) with a FWHM of 10.0 eV describing the profile tails. To be compared with the experimental RRS spectra, the theoretical profiles were convolved with the beam energy profile and experimental broadening of the spectrometer. The theoretical RRS amplitudes were scaled to match the experimental intensities with the same scaling factor for all spectra. Results of these calculations are presented in Fig. 1. As shown, the theoretical shapes are generally in good agreement with the

measured ones, demonstrating that the Kramers-Heisenberg approach reproduces fairly well the RRS spectra in a broad range of x-ray energies. In Fig. 2, the four most intense x-ray RRS experimental spectra induced by photon beams tuned below the K edge are plotted on the same scale, highlighting the evolution of the RRS spectral features as a function of the beam energy. It can be seen that the low-energy tails of the measured RRS spectra merge together into a single curve. This observation, which is expected from theory, is of practical importance for TXRF applications.

A more detailed comparison of the theoretical and experimental spectra showed that for incident energies tuned just below the $1s$ edge the measured intensities slightly below the $K\alpha_{1,2}$ fluorescence line were higher than the calculated ones, when assuming the resonant excitation of $1s$ electrons to the continuum in the RRS process. These discrepancies, peaking at about 1836 eV, suggested the existence of additional, beam energy dependent, $1s$-np photoexcitations that were not considered in the calculations. Further calculations including the most probable photoexcitation channel for silicon, namely, the $1s$-$3p$, were therefore performed. The generalized Kramers-Heisenberg formula [10] combining both the bound and the continuum states was employed. Taking into account that the $3p$ electrons in silicon form the valence band with binding energies in the range from 0 to -5 eV [15] that correspond fairly well to the observed $1s$-$3p$ excitations centered at about 1836 eV, we found that the present experiment is sensitive enough to observe the $3p$ valence band structure. The measured evolution of the $1s$-$3p$ excitation as a function of the beam energy is depicted in Fig. 1(b) (filled areas).

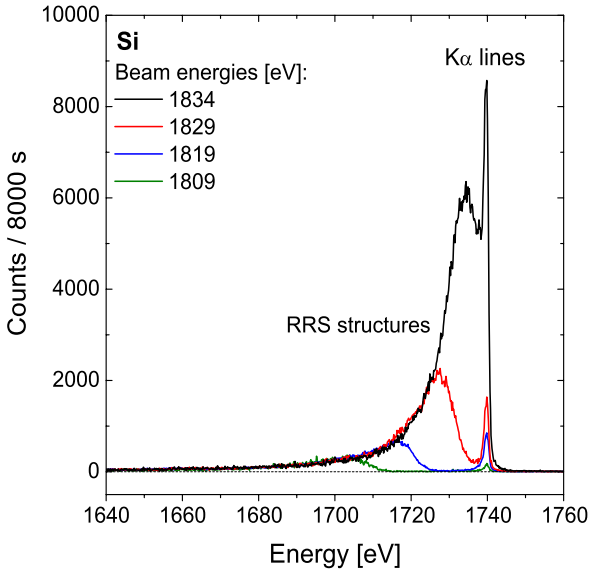

FIG. 2 (color online). X-ray RRS spectra measured at different beam energies below the K edge.

In order to suppress the experimental broadening, the oscillator strength distribution ($dg_{1s}/d\omega$) obtained from the RRS spectra was further deconvolved for the beam energy profile contribution. Adopting a similar deconvolution procedure as the one proposed by Filliponi [16] for extended x-ray-absorption fine structure spectroscopy (EXAFS) applications resulted in an overall resolution of our data of about 3 eV. The deconvolved distribution $dg_{1s}/d\omega$, together with measurements of the linear attenuation coefficients for crystalline and amorphous Si samples taken from [17], is presented in Fig. 3. In fact, both the x-ray-absorption near edge structure in the near edge region (1840–1855 eV) reflecting the distribution of electronic states in the continuum and the EXAFS oscillations occurring above 1855 eV could be extracted. The observed differences between the amorphous, polycrystalline, and crystalline samples can be attributed to the electron scattering effects reported in [18]. We wish to emphasize that, due to the extremely low cross section of the RRS process, the possibility to obtain EXAFS-like information from RRS measurements for silicon at the K edge had not been demonstrated experimentally beforehand.

The total cross sections for the RRS process were derived from the experimental intensities of the integrated x-ray RRS spectra normalized to the intensity of the $K\alpha_{1,2}$ x-ray fluorescence line measured at a beam energy of 1895 eV. The K-shell photoionization cross section at 1895 eV calculated with the XCOM code [19] was adopted for the normalization and the partial fluorescence yield of the $K\alpha_{1,2}$ transitions was taken from [20]. The same method of normalization was employed to determine the cross section for the $1s$-$3p$ excitation. All x-ray yields were

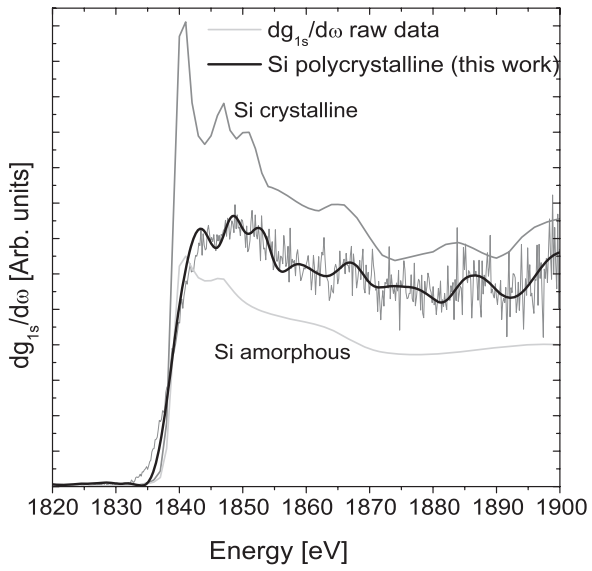

FIG. 3. The oscillator strength distribution $dg_{1s}/d\omega$ obtained from the present RRS measurements for polycrystalline Si compared with the linear attenuation coefficient for amorphous and crystalline Si (from [17]).

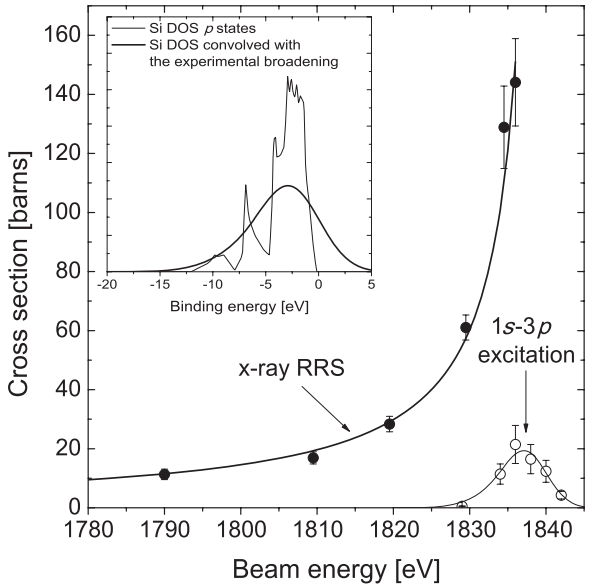

FIG. 4. Measured total cross sections for the Si x-ray RRS (solid circles) and 1s-3p excitation (open circles) plotted versus the incident photon beam energies. The theoretical RRS predictions are shown by the solid line. Inset shows the density of p states in Si (thin line) convolved with our experimental resolution (thick line). The latter was fitted to the evolution of the observed 1s-3p excitation.

corrected beforehand for the differences in the self-absorption in the solid Si target of the incident photons and the emitted ones, whereas the crystal reflectivity and CCD efficiency were assumed to be constant over the energy interval covered by our experiment.

The measured total x-ray RRS cross sections are presented as a function of the incident beam energy in Fig. 4. The theoretical RRS cross sections were obtained by integrating the Kramers-Heisenberg formula (see Ref. [10]) over the energy of the emitted photons. As shown, a quite satisfactory agreement is observed. Other experimental data concerning x-ray RRS cross sections, obtained using different techniques, exist only for the photon beam energy of 1740 eV [21,22]. For the purpose of comparison to these former data, the curve corresponding to the least-squares fit to our results (see Fig. 4) was extrapolated to 1740 eV. A value of 5.41 ± 0.61 b, i.e., $68.1 \pm 7.7\,[r_0^2]$ (where r_0 stands for the classical electron radius) was found, in good agreement with the experimental values of $58 \pm 20\,[r_0^2]$ and $67 \pm 8\,[r_0^2]$ reported in [21,22], respectively, and with the theoretical prediction of $61[r_0^2]$ given by Åberg and Tulkki [7].

The x-ray intensities resulting from 1s-3p excitation were fitted with a theoretical profile obtained from the density of states (DOS) for Si [15] (inset of Fig. 4). The DOS spectrum was convolved with the known experimental broadening and transformed to a beam energy scale assuming an energy of 1840.1 eV [12] for the 1s edge, which corresponds to 0 eV in the DOS curve. Here, we would like to point out that no preedge structure was observed by now for Si in near edge x-ray absorption measurements, most probably because of the very small relative intensity (3%) of 1s-3p photoexcitation process compared to the x-ray fluorescence.

In conclusion, the x-ray RRS spectra of Si were measured for the first time by means of high-resolution x-ray spectroscopy. The overall shapes of the observed x-ray RRS spectra were found to be satisfactorily reproduced by calculations based on the Kramers-Heisenberg formalism. The total x-ray RRS cross sections at the Si K edge were determined and the oscillator strength distribution for continuum states was derived, revealing fine details of the electronic structure of silicon. The weak 1s-3p photoexcitation was observed in silicon for the first time. Finally, it has to be noted that the obtained results are of prime importance for applications of the TXRF technique, which represents the most sensitive method to determine the low-level impurities in Si wafers.

The authors would like to thank Dr. R. Tucoulou and his collaborators at the ESRF beam line ID21 for providing our experiment with very good beam conditions. They also acknowledge the financial support of the Swiss National Science Foundation and the ESRF.

[1] C. J. Sparks, Phys. Rev. Lett. **33**, 262 (1974).
[2] P. Eisenberger, P. M. Platzman, and H. Winick, Phys. Rev. Lett. **36**, 623 (1976).
[3] R. Klockenkämper, *Total Reflection X-Ray Fluorescence Analysis* (Wiley, New York, 1997).
[4] K. Baur *et al.*, J. Appl. Phys. **88**, 4642 (2000).
[5] K. Baur *et al.*, Spectrochim. Acta, Part B **56**, 2049 (2001).
[6] M. Gavrila, Phys. Rev. A **6**, 1348 (1972).
[7] T. Åberg and J. Tulkki, *Atomic Inner-Shell Physics* (Plenum Press, New York, 1985), pp. 419–463.
[8] F. Gel'mukhanov and H. Ågren, Phys. Rep. **312**, 87 (1999).
[9] A. Kotani and S. Shin, Rev. Mod. Phys. **73**, 203 (2001).
[10] J. Tulkki and T. Åberg, J. Phys. B **15**, L435 (1982).
[11] J. Hoszowska *et al.*, Nucl. Instrum. Methods Phys. Res., Sect. A **376**, 129 (1996).
[12] R. D. Deslattes *et al.*, Rev. Mod. Phys. **75**, 35 (2003).
[13] J. L. Campbell and T. Papp, At. Data Nucl. Data Tables **77**, 1 (2001).
[14] H. Hayashi *et al.*, Chem. Phys. Lett. **371**, 125 (2003).
[15] P. S. Fowles *et al.*, Phys. Rev. B **48**, 14 142 (1993).
[16] A. Filliponi, J. Phys. B **33**, 2835 (2000).
[17] A. Owens, G. Fraser, and S. Gurman, Radiat. Phys. Chem. **65**, 109 (2002).
[18] A. Bianconi *et al.*, Phys. Rev. B **36**, 6426 (1987).
[19] http:/physics.nist.gov/xcom.
[20] F. B. Larkins, At. Data Nucl. Data Tables **20**, 311 (1977).
[21] J. M. Hall *et al.*, Phys. Rev. A **19**, 568 (1979).
[22] A. G. Karydas (private communication).